Stationary and transient divertor heat flux profiles and extrapolation to ITER

A. Herrmann [a,*], T. Eich [a], S. Jachmich [d], M. Laux [a], P. Andrew [b],
A. Bergmann [a], A. Loarte [c], G. Matthews [b], J. Neuhauser [a],
ASDEX Upgrade team, Contributors to EFDA-JET work programme

[a] *Max-Planck Institut für Plasmaphysik, Boltzmannstr 2, EURATOM-IPP Association, Garching and Greifswald, Garching 85084, Germany*
[b] *EURATOM-UKAEA Fusion Association, Culham Science Centre, Abingdon, Oxfordshire, UK*
[c] *EFDA-CSU, Max-Planck Institut für Plasmaphysik, Garching, Germany*
[d] *Laboratory for plasma physics, Ecole Royale Militaire, Brussels, Belgium*

Abstract

Experimental results on divertor heat load measurements from ASDEX Upgrade and JET are discussed. Thereby three topics are considered: (i) parameter dependence of steady state heat flux profiles, (ii) spatial distribution of the heat flux profile during type I edge localised modes (ELMs), and (iii) temporal evolution of the energy deposition during type I ELMs. No clear scaling of steady state heat flux profiles with plasma parameters is found. For different data sets a broadening of the heat flux profiles, a constant profile width, as well as a steepening with heating power is found. Extrapolation to ITER requires a review of the data. The heat flux profile is not significantly broadened during type I ELMs. Advantageous is the change of the in/out symmetry. The temporal behaviour of the energy deposition shows a strong increase of the heat flux on time scales of the ion sound speed and an exponential decay with about twice the rise time.
© 2003 Elsevier Science B.V. All rights reserved.

Keywords: Divertor; Heat flux; Edge transport; ELMs; ASDEX Upgrade; JET

1. Introduction

The power handling capability is a crucial problem in toroidal magnetic confinement fusion devices. Present poloidal divertor tokamak experiments are running with a few tens of MW heating power, and the next step device ITER is designed as an experiment with >100 MW of alpha particle heating. A significant part of the heating power is lost by conductive and convective heat transport. Having crossed the separatrix, this power is transported along field lines to the divertor. This parallel heat flux is in the order of a few hundred MW/m^2 in present machines and will be a few GW/m^2 for ITER. The surface temperature of the divertor target material has to be kept below the melting point and the sublimation temperature, respectively, even during short heat bursts. In addition, the averaged heat flux should not exceed the technological feasible maximum of 10 MW/m^2. Both tasks require maximising the area of power deposition by target tilting and flux expansion. The maximum target heat flux can be reduced this way by about a factor of 50 compared to the parallel heat flux.

The shape of the target heat flux profiles is determined by the competition of parallel and perpendicular heat and particle transport in the scrape of layer (SOL). Target heat flux profiles are measured with high temporal resolution by fast infra red (IR) systems and

---

[*] Corresponding author. Fax: +49-89 3299 2580.
E-mail address: albrecht.herrmann@ipp.mpg.de (A. Herrmann).

Langmuir probes. Thermocouple measurements are used at JET to derive a time-averaged heat flux profile in dedicated experiments. The profile shape dependence on global and local plasma parameters has been investigated in many tokamak experiments. Here the main focus is on ITER relevant discharges with an H-mode edge and type I edge localised modes (ELMs). Whereas the good energy confinement of the H-mode is a prerequisite for successful ITER operation, the accompanying type I ELMs are a serious problem.

This paper is organized as follows. After a short discussion of the experimental tools to measure divertor heat flux profiles in Section 2, the behaviour of ELM averaged profiles and scaling laws for the maximum heat flux and the profile width are presented and discussed in Section 3. The energy deposition due to ELMs which is accompanied by a strong temporal variation of the target heat flux resulting in peak heat fluxes of 100 MW/m^2 at ASDEX Upgrade and a few GW/m^2 at JET is discussed in Section 4. Finally, a summary is given. The paper concentrates on experimental results from JET and ASDEX Upgrade. Extrapolation to ITER and its consequences are discussed in the corresponding sections.

2. Diagnostics for divertor heat flux measurements

Different diagnostics and measurement methods are used at ASDEX Upgrade and JET. The diagnostic methods and their results mentioned in this paper are thermography, Langmuir probe measurements and thermometry.

IR systems measuring the photon flux from the target in the near IR region between 3 and 5 μm are used at ASDEX Upgrade and JET. The measured temporal evolution of the surface temperature is used as input for heat flux calculations by solving the 2D heat conduction equation with temperature dependent material parameters. This heat flux to the target represents the sum of heat load by plasma heat conduction and convection, contribution from plasma radiation and neutrals, and the recombination energy of incoming particles. The heat loss due to black body radiation of the target surface is negligible compared to the heat flux necessary to get high surface temperatures on short time scales. The temporal resolution is only limited by the clock rate of the used camera systems, which is typically on the order of 10 MHz resulting in a time resolution of 130 μs/line for the ASDEX Upgrade line camera and about 1 ms/frame for the 2D system at JET. One axis of the 2D array at JET is a time axis because single lines are read out successively, starting in the centre of the array. Assuming toroidal symmetry this results in a maximum time resolution of 21 μs/line. The spatial resolution is between 1 and 2 mm for ASDEX Upgrade and about 5 mm for the JET system.

Langmuir probes, flush mounted in divertor targets, deliver information on the ion flux impinging on the target, the electron temperature and density. The time resolution depends on the measuring mode. Single probe measurements require a scan of the current voltage characteristic and result in a time resolution of a few milliseconds, given by the I–U sweep time. If these characteristics follow standard probe theory, then special arrangements, such as triple probe, can be used for continuous measurement of electron temperature and density, as well as floating potential, with a time resolution restricted by the data acquisition system only. The spatial resolution is limited by the distance between the probe tips, which is a few centimetres, and the poloidal dimension of the probe itself, typically 5–10 mm. The disadvantage of discrete probes can be overcome by plasma sweeping, provided the plasma parameters stay sufficiently constant.

Thermocouple measurements inside divertor tiles are used at JET to derive a time-averaged heat flux profile in dedicated experiments, though with rather restricted time and space resolution. The method presented in [1] measures the energy received by different divertor target tiles during a shot. An average heat flux profile is deduced from a set of identical discharges with the strike point located at different heights of the vertical target of the JET MkIIGB divertor. This method of profile measurements is very expensive in terms of discharges required for a single averaged profile. An improved single shot measurement of an averaged heat flux profile based on thermocouples is presented in [2]. The strike point is shifted slowly, a few ten millimetres per second, over thermocouples embedded in the divertor target. The obtained temporal evolution of the temperature signal inside the bulk material is then modelled by a finite element code with a guessed target heat flux profile as input. The profile is adjusted until the error between the calculated and measured thermocouple traces is minimised.

3. Steady state heat load

Steady state heat flux profiles are routinely measured by thermography in ASDEX Upgrade and in JET, if the strike point position is in the field of view of the IR camera. The variation of the profile shape with discharge parameters is investigated for different divertor geometries, the open DIV I, and the closed DIV II configuration in ASDEX Upgrade, as well as for the MKIIGB divertor in JET. The measured heat flux profiles have a narrow component with an exponential decay close to the maximum and a broader shoulder further away [3]. The e-folding length near the maximum and the maximum heat flux are used for a statistical analysis of about 50 H-mode discharges with type I and

type III ELMs in DIV I configuration of ASDEX Upgrade, resulting in the following scaling for the maximum heat flux and the decay length at the outer target [3]:

$$q_{max}(W\,m^{-2}) = 8.837 \times 10^3 P_{sep}^{0.5 \pm 0.05} \ (W)$$
$$\times q_{95}^{-0.27 \pm 0.3} \bar{n}_e^{-0.77 \pm 0.16} (10^{19} \ m^{-3}),$$

$$\lambda_p(mm) = 6.56 \times 10^{-3} P_{sep}^{0.52 \pm 0.05} \ (W)$$
$$\times q_{95}^{0.7 \pm 0.3} \bar{n}_e^{0.09 \pm 0.17} (10^{19} \ m^{-3}).$$

This scaling reveals that both the maximum heat flux and the decay length increase with the square root of the total power into the divertor. The same power law ansatz used for DIV I was applied to DIV II data. This data set comprises only data with type I ELMs. It results in a nearly linear dependence of the maximum heat flux from the heating power and reveals no broadening of the profile [4]:

$$q_{max} \ (W\,m^{-2}) = 0.114 P_{sep}^{1.1 \pm 0.06} \ (W)$$
$$\times q_{95}^{1.6 \pm 0.6} \bar{n}_e^{-1.0 \pm 0.2} (10^{19} \ m^{-3}),$$

$$\lambda_p \ (mm) = 0.34 \times 10^3 P_{sep}^{-0.07 \pm 0.06} \ (W)$$
$$\times q_{95}^{-1.6 \pm 0.6} \bar{n}_e^{0.6 \pm 0.2} (10^{19} \ m^{-3}).$$

The main difference between the DIV I and DIV II scaling is the dependence on the total divertor power and the profile broadening with density. Reasons for this might be that type III ELM discharges as well as discharges with a partial divertor detachment are included in the DIV I data set. This has to be checked by using a subset of data with type I ELM behaviour and attached divertor conditions. Another physical reason for the different scaling found for DIV I and DIV II might be due to the different divertor geometry. The closed divertor DIV II is designed to reduce the maximum heat flux by a preferential direction for neutrals and desorbed particles against the separatrix, increasing the effective particle density in the hot region near the separatrix. This rather than the profile shape reduces the maximum heat flux.

The data set available at JET is limited to a few discharges with IR optimised strike point position not allowing for a detailed statistical analysis. The heating power and the density (fueling rate) was varied at a constant value of $q_{95} = 3$. Plotting the measured e-folding length versus the heating power shows no increase of the decay length with heating power, as shown in Fig. 1. The expected change of the decay length is on the order of 20% for a square root like dependence due to the comparatively small variation of the heating power, as indicated in Fig. 1. A clear relation between heating power and profile width is not deducible.
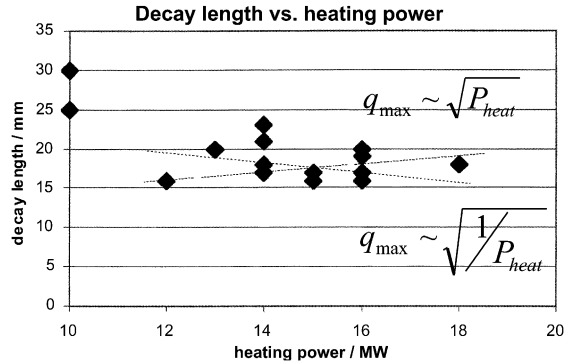

Fig. 1. Variation of near peak e-folding length with heating power at the outer divertor of JET.

A further restriction is the spatial resolution of the system which is comparable with the measured e-folding lengths. The apparatus function is now measured during the in vessel calibration procedure, so that a profile deconvolution can be performed. Nevertheless, an investigation of the parameter dependence of heat flux profiles requires a wider variation of the heating power by at least a factor of 4.

Measurements with thermometrical methods reveal peaked target profiles [1,5] which become steeper with increasing heating power and flatten with increasing density. Whereas the density dependence and the peaked structure of the heat flux profile as measured by thermometry is comparable to the results of thermographic measurements, the profile steepening with about the square root of heating power [5] is not found by thermography. It is concluded from onion skin modelling, 3D Monte-Carlo ion orbit loss modelling (ASCOT code), and Langmuir probe measurements, that the narrow component represents the ion component of heat transport and its behaviour is dominated by ion orbit losses from the pedestal region [5].

A multi-machine scaling of the heat flux decay length mapped to the outer midplane using data from JT-60U, ASDEX Upgrade, DIII-D, and JET, is presented in [6]. The H-mode scaling of data without gas puffing shows a positive dependence on the power to the divertor, $\lambda_q^{H-1} \sim P_{div}^{0.44 \pm 0.04}$.

Theoretically, the heat flux e-folding length (scrape off layer width) is described by a competition of parallel and perpendicular transport so that, for a qualitative discussion, the characteristic thickness of the SOL can be described by: $\Delta_s \sim (\chi_\perp \tau_\parallel)^{1/2}$ where $\tau_\parallel$ is the energy confinement time of the SOL given by the ratio of stored energy in the SOL and the power influx, P_{sep}. $\chi_\perp$ is the perpendicular heat transport coefficient. The SOL-width then becomes [10]: $\Delta_s \sim n_s T_s(\chi_\perp / P_{sep\perp})$. It becomes broader with rising electron pressure at the midplane and rising perpendicular electron heat conductivity. It is

steepened with power crossing the separatrix. In the case of an H mode edge at the pressure gradient limit, i.e. $n_s T_s / \Delta_s = $ const., the perpendicular heat transport coefficient is proportional to the power crossing the separatrix. The profile width then no longer depends explicitly on the heating power. However, depending on the parallel heat transport the separatrix pressure depends implicitly on the heating power.

Despite the fact that a reliable extrapolation of the heat flux e-folding length to ITER requires further investigation, a rough estimation of the target load can be done to give an idea of the expected target heat flux. In the case of a constant profile width of 5 cm at the target and a radiative fraction of 0.7, the resulting target heat flux becomes:

$$q_{\text{target}} = \frac{(1 - 0.7) \times 100}{2\pi \times 6.2 \times 0.05} \approx 15 \text{ MW m}^{-2}.$$

4. Heat flux profiles during type I ELMs

In addition to the steady state divertor load, burst like heat fluxes arrive at the target in discharges with H mode edge due to mhd instabilities, so-called ELMs. Each of these ELMs expels energy from the plasma edge on a hundred microsecond time scale which is then transported to the target plates. This paper illuminates the deposition behaviour of type I ELMs. These types of ELMs are typical for H mode with a pedestal as envisaged for ITER and the energy loss per ELM is a key figure for extrapolation from present machines to ITER because melting or sublimation of the target material has to be avoided. This limits the energy impact during heat bursts to $20–40 MJ/(\text{m}^2 \text{s}^{1/2})$ for carbon and tungsten, respectively [11]. Here we concentrate on the relation between midplane energy loss and deposition at the plate as well as spatial and temporal profiles. Fig. 2 shows the relation between the fraction of plasma energy lost by an ELM and the normalised ELM frequency, $f\tau$. ASDEX Upgrade and JET data are in line, however, they are separated. JET data are found to be at higher values for the ELM energy loss and lower values of the normalised ELM frequency. This means that, because the energy confinement time at JET is higher than at ASDEX Upgrade, the ELM frequency decreases stronger than the energy confinement time increases ($f \sim \tau^{-\alpha}$, $\alpha > 1$), as found experimentally in ASDEX Upgrade [7]. This has to be compensated by a higher ELM energy loss to keep the ELM transported power, $f_{\text{ELM}} \Delta W_{\text{ELM}} / P_{\text{heat}}$, constant. Consequently, expectations for ELM losses in ITER are at values above the JET data. An ELM loss of 10% results in an absolute value for a midplane ELM loss of 30 MJ in ITER. To deposit this energy at the divertor plate without damaging the target requires that the product of wetted area and square root
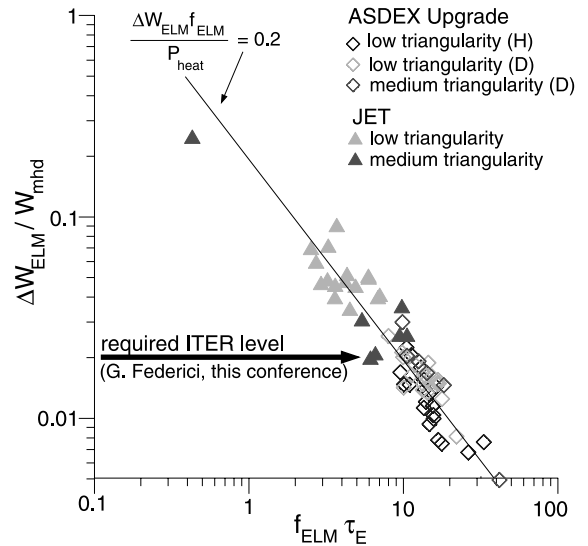

Fig. 2. Variation of midplane losses due to an type I ELM versus normalised ELM frequency for JET and ASDEX Upgrade data.

of the ELM deposition time is $A_{\text{wetted}} \sqrt{\Delta t} > 1 \text{ m}^2 \text{s}^{1/2}$. From this follows, that a reduction of the ELM load can be achieved by increasing the wetted area or by increasing the deposition time or a combination of both. Extrapolation to ITER requires an investigation of both effects separately.

The ratio between midplane losses and target load as well as the distribution between load to the inner and outer target will be discussed first in this section. Then the spatial and temporal distribution of heat load at the targets will be presented followed by a short discussion of ELM transport models and extrapolations to ITER.

The fraction of plasma stored energy deposited per ELM at the target plates of JET and ASDEX Upgrade versus the line averaged density is shown in Fig. 3. The ELM energy is equally distributed between the inner and outer divertor in JET and preferentially deposited to the inner divertor in ASDEX Upgrade with an in/out ratio increasing from 2 to 4 with density. In between ELMs, the ratio is inverted typically to about 0.5 for JET and ASDEX Upgrade [8,9]. This may in principle be advantageous for steady state operation, because a lower base load results in a lower base temperature, so that the tolerable temperature change ($T_{\text{melt}} - T_{\text{base}}$) is higher. The fraction of plasma stored energy deposited during an ELM at the target decreases with density. At ASDEX Upgrade this is correlated with the start of partial divertor detachment. Unfortunately, this decrease of ELM deposited energy is not a result of additional energy loss between midplane and target during an ELM. As shown in Fig. 4, the ratio of energy loss from the core to the
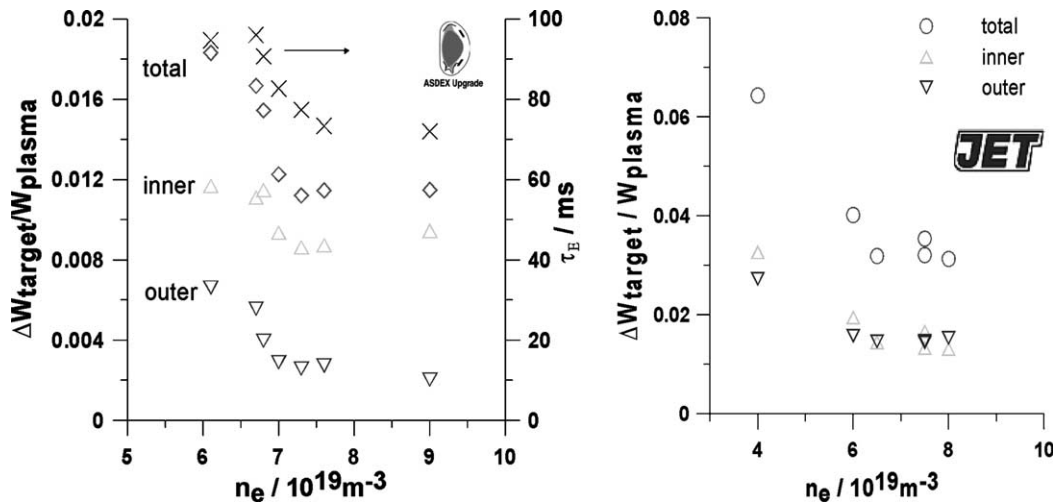
Fig. 3. Fraction of ELM losses at the target in dependence on line averaged density for ASDEX Upgrade (left) and JET (right).
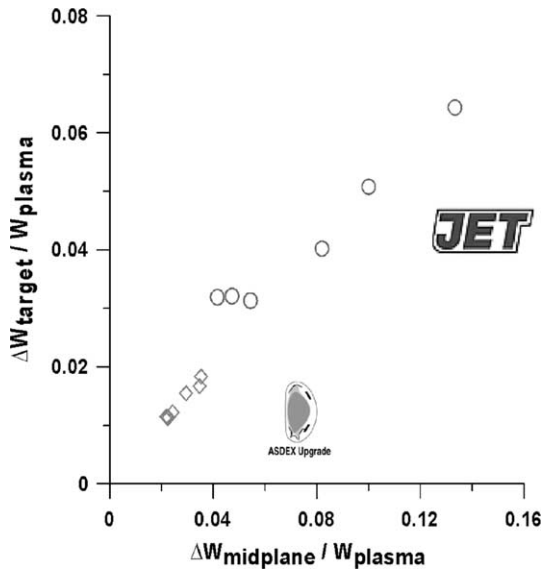

Fig. 4. Ratio of midplane energy loss and target load for JET and ASDEX Upgrade.

energy arriving at the target is constant and independent on the line averaged density. The reduction of the ELM energy deposited at the target only reflects the loss of plasma confinement and energy stored in the pedestal region, respectively.

4.1. Spatial distribution

The heat flux to the outer plate during a type I ELM increases strongly at JET, but less pronounced at AS-DEX Upgrade (Fig. 5). The spatial shape of the profile itself is not changed significantly during the ELM, so

that the ELM effect on the profile at the outer target is just a self-similar increase of the amplitude by a factor between 1.5 and 5. The heat flux profile at the inner plate during a type I ELM shows a pronounced peak near the separatrix with an e-folding length comparable to that at the outer plate [11]. Fig. 6 shows the ratio of decay lengths during and in between ELMs for a set of discharges in the DIV II configuration of ASDEX Upgrade. It includes values from discharges having the outer strike point at the top of the roof baffle, which corresponds to an open divertor geometry as well as configurations with the strike point at the vertical target, i.e. the closed situation. The lines in Fig. 6 span a space of profile broadening between a factor of 1 and 2. This region includes most of the data points. This means that profile broadening is not a significant effect for the reduction of the ELM impact.

If discussed in terms of diffusive transport, this profile stiffness means, that the ratio of parallel to perpendicular heat transport, as discussed in Section 2 for steady state transport, is kept constant. This is qualitatively understandable assuming Bohm like transport: a higher electron temperature in the midplane increases on the one hand the perpendicular heat transport coefficient and on the other hand reduces the parallel transport time for energy in the SOL.

The position of the maximum heat flux at the outer target is rather constant in ASDEX Upgrade as well as in JET. The inner strike point is found to move inwards in JET up to 20 cm in discharges with high loss of plasma stored energy (hot ion H-mode, giant ELMs [12]). It is assumed, that the strike point movement is due to a change of the magnetic field topology in the divertor [12]. In principle, such a jump can help to increase the tolerable amount of deposited energy by the effect that the heat is deposited temporarily in a region
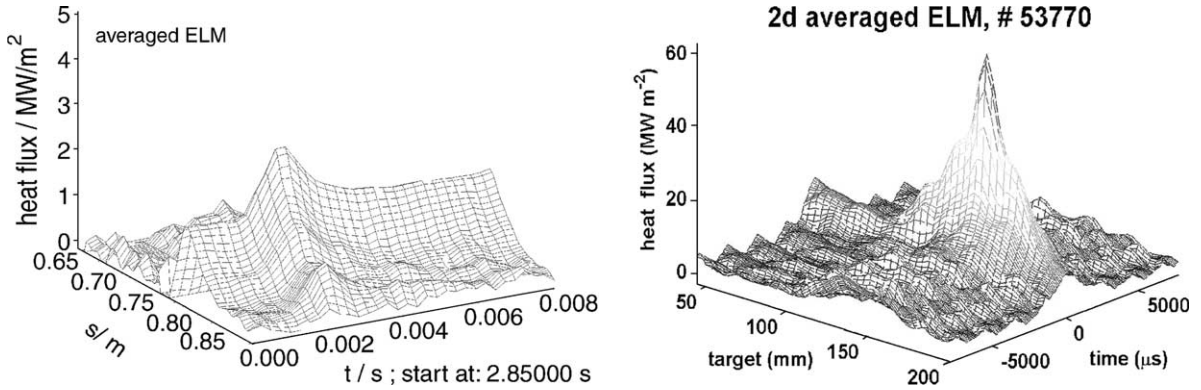
Fig. 5. Temporal behaviour of a type I ELM in ASDEX Upgrade (left) and JET (right).
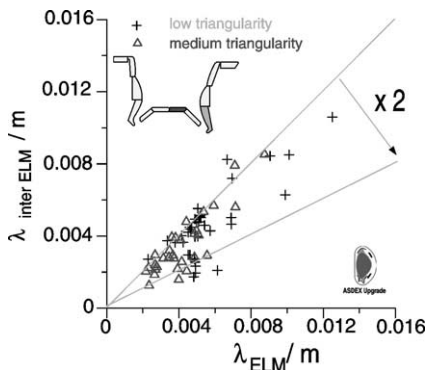

Fig. 6. Midplane inter ELM decay lengths compared to the decay lengths between ELMs as measured in ASDEX Upgrade.

with a lower base load and consequently a lower steady state temperature. But, because the steady state surface temperature is less than half of the maximum tolerable surface temperature, the achievable increase factor for the tolerable energy load is below two.

4.2. Temporal behaviour

Whether or not the ELM duration becomes shorter with machine size is essential to predict the tolerable load to the ITER divertor. The heat flux deposition pattern in ASDEX Upgrade and JET is characterised by the total energy deposited to the target and the ELM rise time, i.e. the time duration between the start of the ELM and the ELM maximum. These values depends only weakly on assumptions made in the model for heat flux calculation in contrast to the calculated maximum heat flux which can vary by a factor of 10 [13,14]. Conclusions drawn from the temporal decay of the energy deposition have to be verified against other fast measurements, such as ion saturation current from Langmuir probes. A comparison between Langmuir

probes and thermography is shown for ASDEX Upgrade in Fig. 7. In a first phase strong fluctuations of the measured ion saturation current are found. This phase lasts about 500 μs which corresponds to the rise time for the maximum heat flux measured by thermography. The decay of the heat flux, as well as the ion saturation current can be characterised by an e-folding time of 1–2 ms. This means that the ratio of energy deposited before the maximum to that deposited after maximum is comparable.

The pronounced fluctuation phase during the ELM deposition as observed at ASDEX Upgrade is absent at JET. Therefore, one can derive the temporal evolution of the electron temperature and the floating potential from Langmuir measurements as shown in Fig. 8. Floating potential and electron temperature show a fast increase with the ELM onset followed by a delayed raise of the ion saturation current. This behaviour is qualitatively modelled by particle in cell calculations [16] and a 1-D SOL transport code (SOL-one) [15]. During the ELM electrons are nearly collisionless and the transport becomes essentially sheath limited. The ions arrive on a time scale of the ion sound speed and transfer most of the energy to the target as shown in Fig. 9.

Simpler ELM models to describe the fraction of plasma losses by an ELM are based on the competitive process of energy release on a short mhd time scale across field lines in the midplane and parallel transport to the target [17–19]. The relation between the characteristic time for the energy flow to the target and the ELM rise time as measured by thermography is shown in Fig. 10. Here, the characteristic time is calculated as collisionless transport of ions with the sound speed calculated from pedestal values of electron temperature. The collisional term for the parallel transport is neglected. If the collisional term would be included the characteristic transport time for ASDEX Upgrade would be higher because the pedestal is collisional in contrast to JET. Using the collisonless ion flow time as
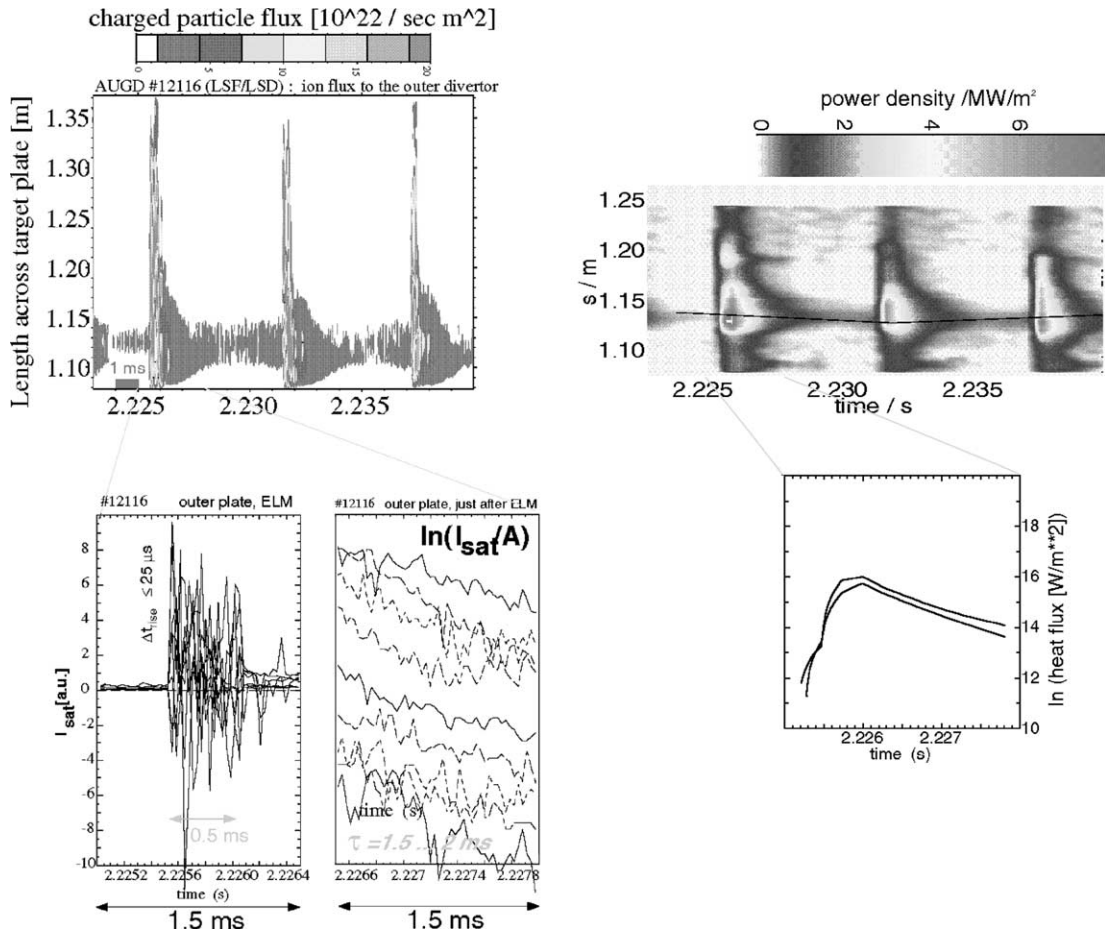
Fig. 7. Ion saturation current measured by Langmuir probes (left) and heat flux profile measured by thermography (right) in ASDEX Upgrade results in a comparable time scale for the ELM rise time and the decay.
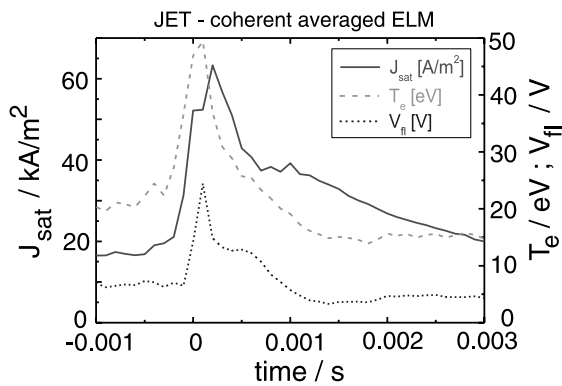

Fig. 8. Temporal evolution of ion saturation current, electron temperature, and floating potential for type I ELM at the outer target plate in JET.
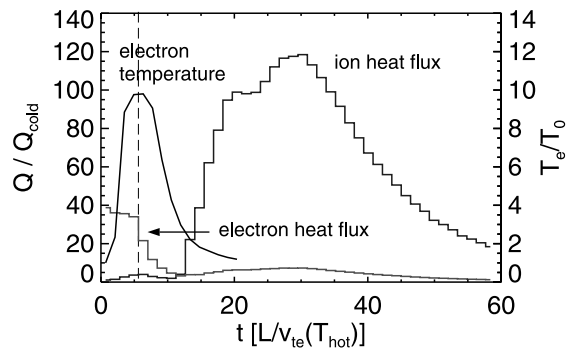

Fig. 9. PIC code calculation for burst like energy transport from the midplane to target plates. The values are normalised to the values in the SOL before the ELM. The vertical dashed line marks the end of the ELM pulse in the midplane.

characteristic parallel transport time unifies the relation between ELM rise time and parallel transport time for

JET and ASDEX Upgrade as shown in Fig. 10. The expected ELM energy loss in ITER depends on whether
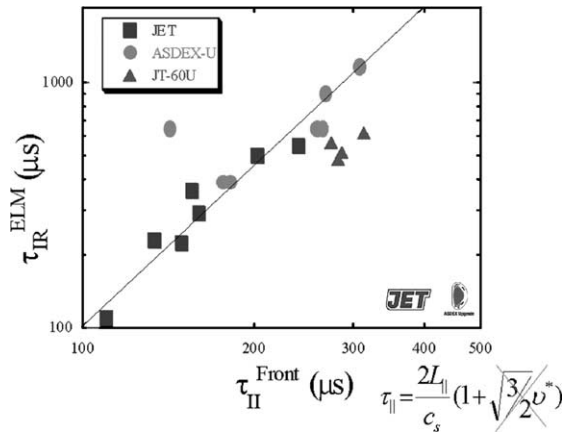
Fig. 10. ELM rise time as measured by thermography compared to the parallel transport time for ions calculated from pedestal temperature and density of electrons.

Table 1
Estimation of type I ELM energy impact at the outer target for ITER

		5 [Ref. 20]
Midplane energy loss (MJ)	30	5 [Ref. 20]
Energy deposited at the outer target (MJ)	15	2.5
Energy deposited in the first phase of the ELM (MJ)	7.5	1.25
Wetted area $2\pi \times 6.2 \times 0.05$ (m^2)	1.9	1.9
...with broadened profile (m^2)	3.8	3.8
ELM rise time (Fig. 6 in [20] and Fig. 10) (s)	500	500
Energy impact (MW/(m^2 s$^{0.5}$))	88	14

The assumed midplane losses represents a pessimistic and an optimistic extrapolation.

or not the collisional term has to be included in the calculation of the energy transport time. The fractional ELM losses are less for ITER, if the transport scales with the ion flow time [20].

The implications for ITER are summarised in Table 1 for two different midplane energy losses, a decay length of 0.05 m at the outer target, and profile broadening during the ELM by a factor of two.

5. Summary

Steady state heat flux profiles at the outer plate in ASDEX Upgrade and JET were characterised by the maximum heat flux and an e-folding length fitted to the profile near the separatrix. The e-folding length becomes broader with the square root of heating power for the data set of the open divertor DIV I, including type I and type III ELMs, and stays about constant for the purely

type I ELM data set of DIV II in ASDEX Upgrade. Correspondingly, the maximum heat fluxes scales with the square root and linear with heating power, respectively. The limited number of JET data did not allow to find a clear power dependence for the profile width from thermography data. Data from thermometry point to a steepening of the profile width in low density discharges, which is attributed to a fast ion component for this low collisionality case. A reliable extrapolation to ITER requires to improve the data sets used for the scaling. Assuming a constant profile width would result in steady state heat fluxes of about 15 MW/m^2 in ITER, which is marginally at the technological limit.

The relation between ELM energy losses in the midplane and energy load to the target is linear over a wide density range. The asymmetry of energy deposition is changed from an in/out ratio of about 0.5 for the steady state profiles to a balanced situation in JET (in/out = 1) and preferential inward deposition in ASDEX Upgrade (in/out = 2 to 4). The broadening of the profile is below a factor of two for both experiments.

The temporal behaviour of type I ELM energy deposition has been simultaneously measured by thermography and Langmuir probes. The ELM rise time and heat flux decay turn out to be comparable for both methods. The ELM decay time is larger than the ELM rise time, so that a part of the ELM energy is deposited after the heat flux maximum and has not to be considered for the energy impact.

A significant part of the ELM energy is deposited to the inner target which can tolerate a higher energy impact due to the lower time averaged heat deposition. This effect and the temporal behaviour of the deposition profile result in a reduction of the midplane loss to be considered for the energy impact at the target by a factor of 4 in maximum. The estimated energy impact for type I ELMs in ITER is 88 and 14 MJ/(m^2 s$^{0.5}$), respectively.

The mechanism of energy transfer from the midplane to the target has been qualitatively described by particle in cell calculations as well as a simple 1D SOL transport code. Fast electrons reaching the target nearly collisonless results in a fast increase of the sheath potential and sheath limited parallel transport. The major part of the energy is transported by ions on a time scale of the ion sound speed. Correlating this parallel ion transport time with pedestal data results in the same dependence for ASDEX Upgrade and JET data. This has implications for simple ELM transport models and extrapolation to ITER, as discussed in [20].

References

[1] G. Mathews et al., J. Nucl. Mater. 290–293 (2001) 668.
[2] V. Riccardo et al., Plasma Phys. Control. Fusion 43 (2001) 881.

[3] A. Herrmann et al., in: Proceedings of 23rd European Conference, Kiev, 1996, Controlled Fusion and Plasma Physics, vol. 20C, Part II, 1996, p. 807.

[4] A. Herrmann et al., in: Proceedings of 25th European Conference, Praha, 1998, Controlled Fusion and Plasma Physics, vol. 22C, 1998, p. 488.

[5] W. Fundamenski et al., in: Proceedings of 28th European Conference, Madeira, 2001, Controlled Fusion and Plasma Physics, Or. 13.

[6] A. Loarte et al., J. Nucl. Mater. 266–269 (1999) 587.

[7] A. Herrmann et al., in: Proceedings of 27th European Conference, Budapest, 2000, Controlled Fusion and Plasma Physics, vol. 24B, 2000, p. 1180.

[8] A. Herrmann et al., Plasma Phys. Control. Fusion 37 (1995) 17.

[9] T. Eich et al., these Proceedings. PII: S0022-3115(02)01477-0.

[10] P.J. Harbour, Nucl. Fusion 24 (1984) 1211.

[11] A. Herrmann, Plasma Phys. Control. Fusion 44 (2002) 883.

[12] J. Lingertat et al., in: Proceedings of 22nd European Conference, Bornemouth, 1995, Controlled Fusion and Plasma Physics, vol. 19C Part III, 1995, p. 281.

[13] A. Herrmann, in: Proceedings of 28th European Conference, Madeira, 2001, Controlled Fusion and Plasma Physics, P.5.104.

[14] P. Andrew et al., these Proceedings. PII: S0022-3115(02)01586-6.

[15] J. Lingertat et al., J. Nucl. Mater. 241–243 (1997) 402.

[16] A. Bergmann, Nucl. Fusion 42 (2002) 1162.

[17] G. Janeschitz et al., J. Nucl. Mater. 290–293 (2001) 1.

[18] A. Loarte et al., in: Fusion Energy 2000, ITERP/11(R), Proceedings of 18th IAEA Fusion Energy Conference, Sorrento, Italy, 2000, IAEA, Vienna 2001, ISSN 1562-4153.

[19] Yu. Igitkhanov et al., in: Proceedings of 28th European Conference, Madeira, 2001, Controlled Fusion and Plasma Physics, P.4.101.

[20] A. Loarte, these Proceedings. PII: S0022-3115(02)01398-3.